

Automated synthesis of oxygen-producing catalysts from Martian meteorites by a robotic AI chemist

Received: 11 March 2023

Accepted: 27 September 2023

Published online: 13 November 2023

 Check for updates

Qing Zhu^{1,8}, Yan Huang^{1,8}, Donglai Zhou^{1,8}, Luyuan Zhao^{1,8}, Lulu Guo¹, Ruyu Yang¹, Zixu Sun¹, Man Luo¹, Fei Zhang², Hengyu Xiao¹, Xinsheng Tang², Xuchun Zhang², Tao Song², Xiang Li², Baochen Chong², Junyi Zhou², Yihan Zhang², Baicheng Zhang¹, Jiaqi Cao¹, Guozhen Zhang¹, Song Wang¹, Guilin Ye³, Wanjun Zhang³, Haitao Zhao⁴, Shuang Cong², Huirong Li¹, Li-Li Ling⁵, Zhe Zhang^{5,6}, Weiwei Shang²✉, Jun Jiang^{1,7}✉ & Yi Luo^{1,7}✉

Living on Mars requires the ability to synthesize chemicals that are essential for survival, such as oxygen, from local Martian resources. However, this is a challenging task. Here we demonstrate a robotic artificial-intelligence chemist for automated synthesis and intelligent optimization of catalysts for the oxygen evolution reaction from Martian meteorites. The entire process, including Martian ore pretreatment, catalyst synthesis, characterization, testing and, most importantly, the search for the optimal catalyst formula, is performed without human intervention. Using a machine-learning model derived from both first-principles data and experimental measurements, this method automatically and rapidly identifies the optimal catalyst formula from more than three million possible compositions. The synthesized catalyst operates at a current density of 10 mA cm⁻² for over 550,000 s of operation with an overpotential of 445.1 mV, demonstrating the feasibility of the artificial-intelligence chemist in the automated synthesis of chemicals and materials for Mars exploration.

Mars has for decades attracted intensive scientific exploration and research in countries worldwide. Finding signs of past life and building potentially habitable regions on Mars have long been a dream of humanity. In situ resource utilization on Mars will be applied to substantially reduce the cost and complexity of human missions, enabling sustainable exploration by utilizing local resources to produce necessary supplies. Oxygen supply must be the top priority for any human

activity on Mars, because rocket propellants and life support systems consume substantial amounts of oxygen, which cannot be replenished from the Martian atmosphere^{1,2}. Fortunately, recent evidence of water activity^{3,4} has raised the prospect of large-scale oxygen production on the planet through solar-power-driven electrochemical water oxidation processes using an oxygen evolution reaction (OER) catalyst. Using extraterrestrial catalysts developed from local materials to drive

¹Key Laboratory of Precision and Intelligent Chemistry, Hefei National Research Center for Physical Sciences at the Microscale, School of Chemistry and Materials Science, University of Science and Technology of China, Hefei, China. ²School of Information Science and Technology, University of Science and Technology of China, Hefei, China. ³Hefei JiShu Quantum Technology Co. Ltd., Hefei, China. ⁴Materials Interfaces Center, Shenzhen Institute of Advanced Technology, Chinese Academy of Sciences, Shenzhen, China. ⁵Deep Space Exploration Laboratory, Hefei, China. ⁶School of Aerospace Engineering, Beijing Institute of Technology, Beijing, China. ⁷Hefei National Laboratory, University of Science and Technology of China, Hefei, China. ⁸These authors contributed equally: Qing Zhu, Yan Huang, Donglai Zhou, Luyuan Zhao. ✉e-mail: wshang@ustc.edu.cn; jiangj1@ustc.edu.cn; yiluo@ustc.edu.cn

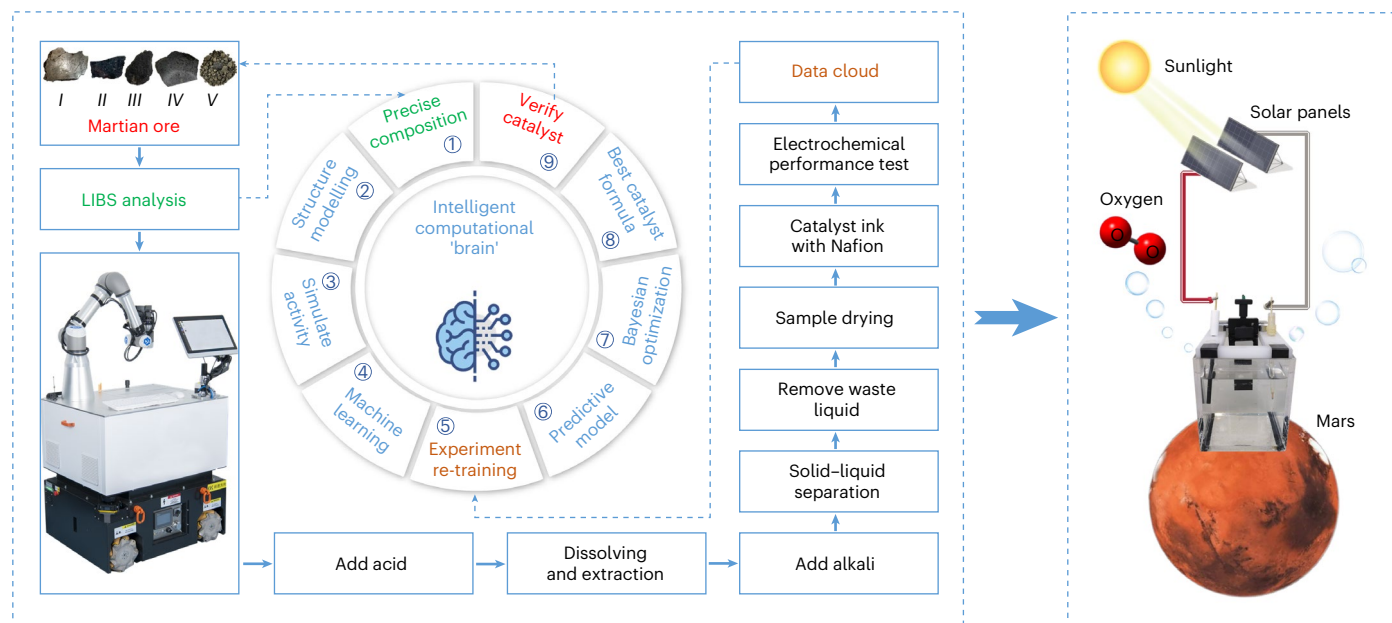


Fig. 1 | Workflow of an all-encompassing system for the on-site design and production of an OER electrocatalyst on Mars by an AI chemist consisting of a mobile robot, a computational 'brain', a cloud server and 14 task-specific workstations. The dual-cycle automated process integrates material preparation, catalyst production, performance characterization and formula optimization in the following steps, as labelled. Step 1: Analyse the precise composition of Martian ores by LIBS. Step 2: Generate polymetallic catalyst structures by classical MD simulations. Step 3: Calculate the OER activities

of the structures using DFT. Step 4: Build an NN model using simulation data. Step 5: Re-train the NN model using robotic experimental data. Step 6: Fine-tune the parameters in the NN model to predict experimental overpotential with confidence level over 0.95. Step 7: Screen for the optimum formula using Bayesian optimization algorithms. Step 8: Predict the optimal synthetic formula with the lowest OER overpotential using available Martian ores. Step 9: Validate the OER performance of the catalyst prepared with predicted formula (arrow pointing back to 'Martian Ore' box for feedstocks configuration).

oxygen production allows for the on-site production of fuel and oxygen on Mars, which represents a low-hanging fruit in the exploration of this planet. However, two major technical challenges must be overcome to synthesize usable OER catalysts by using local Martian raw materials^{5,6}. First, the synthetic system must be unmanned and self-directing, as the vast astronomical distance hinders real-time remote guidance from humans. Second, it should be equipped with the scientific intelligence needed to efficiently identify the best formula of catalyst ingredients through artificial-intelligence (AI) algorithms, given knowledge of elemental abundances in the Martian local ores. Designing a catalyst from a given list of elements requires the exploration of a vast chemical space, which poses a daunting task using the conventional 'trial-and-error' paradigm. Given five different local Martian ores as feedstocks, there are 3,764,376 possible formulas, estimated by the combination of integer percentages in 1% intervals; finding the optimal formula would require 2,000 years of human labour to finish such a screening, where each complete experiment takes 5 hours, at least.

Robotic synthetic systems with AI appear to be the only viable technology for addressing these two challenges, as suggested by recent advances in automated chemical synthesis systems. The mobile chemist by Cooper and colleagues shows excellent ability to perform high-throughput performance testing for human-made photo-catalysts, providing local optimization with measured data to achieve better formulations⁷. The ChemPU system by Cronin and colleagues demonstrates its extraordinary power in automatic synthesis of organic molecules starting from machine-reading synthetic chemistry literature⁸. These robotic systems need an intelligent subsystem to acquire chemical knowledge and form predictive physical models to direct local optimization in chemical synthesis. Inspired by these researchers' pioneering work on robotic chemical synthesis systems, we have developed an all-in-one robotic artificial-intelligence chemist (AI chemist) to enable automated, self-directed synthesis. Not only can it conduct the

entire process of chemical synthesis, structural characterization and performance testing using a mobile robot and 14 task-specific chemistry workstations but it can design the best formula for a chemical synthesis task through a powerful computational module that combines machine learning (ML) algorithms and theoretical models to analyse both robot-acquired experimental data and massive first-principles simulation data⁹. Our AI chemist has accelerated the discovery of the optimal synthetic formulas for high-entropy electrocatalysts by five orders of magnitude compared to conventional trial-and-error experiment paradigm. Without prior knowledge about the exact composition of available Martian ores for making OER catalysts, the proposed automated approach must not only be capable of screening numerous candidates for the best formula, but also be intelligent to dissect usable yet unidentified raw materials and determine the predictive model on-the-fly. We developed a specific protocol for our AI-chemist system to tackle this challenge, advancing the in situ resource utilization strategy for Mars and interstellar exploration in the future.

In this proof-of-concept work, we demonstrate the superiority of the data-driven protocol using an AI chemist over the conventional trial-and-error protocol by the design of a six-metallic element OER catalyst from a pool of 3,764,376 compositions. Within six weeks, the AI chemist built a predictive model by learning from nearly 30,000 theoretical datasets and 243 experimental datasets using ML and Bayesian optimization algorithms, which delivers a promising OER catalyst formula coupled with the most suitable synthetic conditions. The resulting polymetallic material (comprising Mn, Fe, Ni, Mg, Al and Ca) catalysed the OER with an overpotential of 445.1 mV at a current density of 10 mA cm⁻², maintained for 550,000 s. Further, the stress test at -37 °C, which mimics the temperature condition on Mars, confirmed that it can steadily produce oxygen without apparent deterioration, suggesting that it can work in the harsh conditions on Mars. A ground-based verification system is currently being developed to provide more

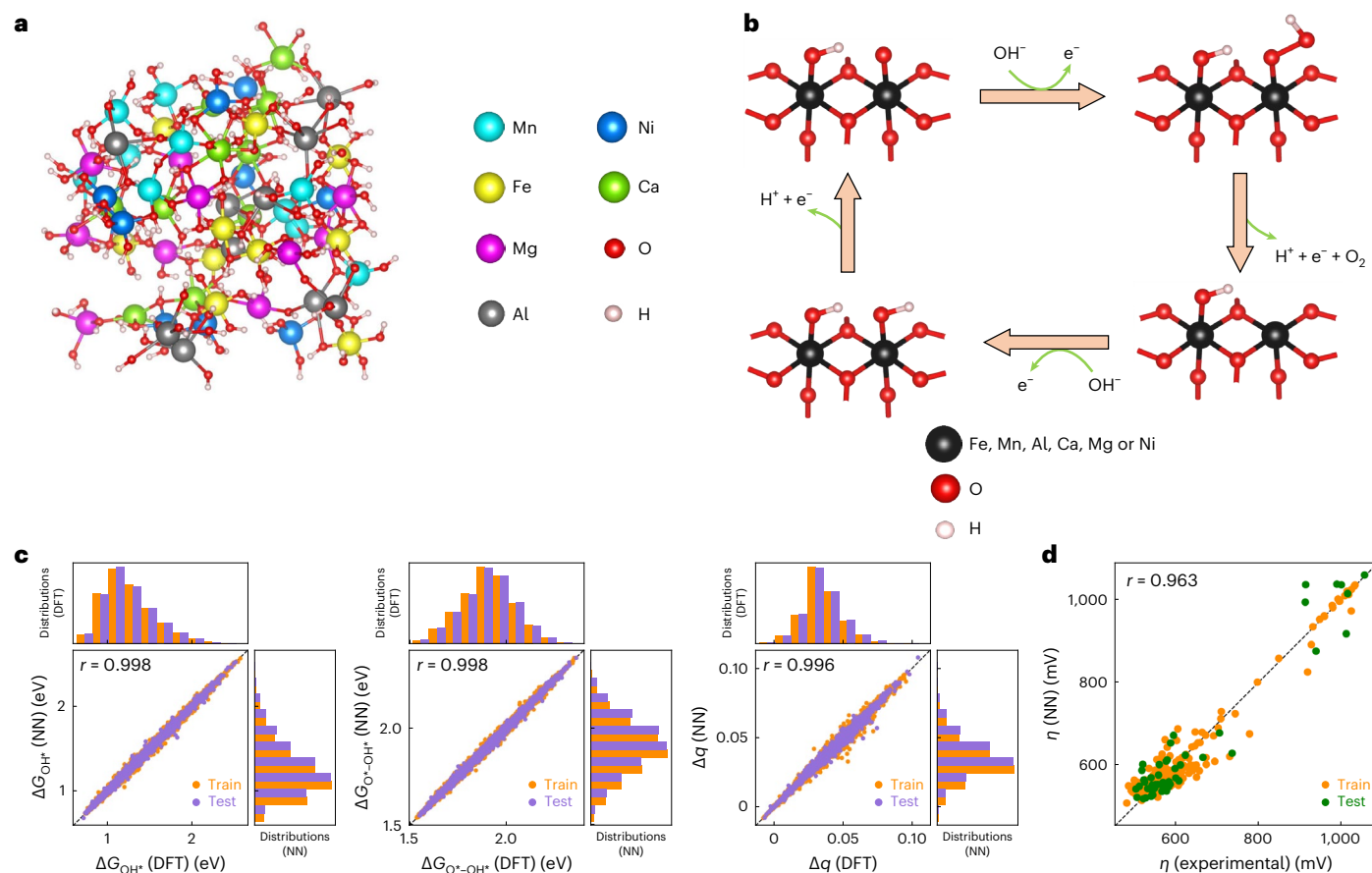


Fig. 2 | Theoretical simulation and performance prediction of multimetallic hydroxides. **a**, Representative structure of multimetallic hydroxides generated by classical MD simulation. **b**, Reaction mechanism of the OER. **c**, Statistics

of three OER descriptors, $\Delta G_{\text{OH}\cdot}$, $\Delta G_{\text{O}\cdot-\text{OH}\cdot}$ and Δq , predicted by the NN. **d**, The prediction results of measured OER overpotentials by predictive model that was calibrated by experiments. In **c** and **d**, r is the Pearson correlation coefficient.

realistic space conditions for the AI chemist, which will be essential for the construction of the International Lunar Research Station and Mars Research Station; both were designed for long-term robotic operation and short-term human participation. The AI chemist thus represents a promising technique for on-site synthesis of OER electrocatalysts on Mars and constitutes a versatile and efficient platform for the supply of complex functional materials for planetary and space exploration.

Protocol for the AI chemist making OER electrocatalysts on Mars

To facilitate the work of the AI chemist on Mars, we proposed a double-layer workflow for the on-site synthesis of OER electrocatalysts (Fig. 1). The outer layer, which comprises a 12-step automated experiment and data management, is done by the robot and various ‘smart’ chemical workstations; the inner layer, which includes nine consecutive digital operations, is executed by the intelligent computational ‘brain’ (Supplementary Video 1 and Supplementary Figs. 1–3).

In the experimental cycle, samples of local ore (Supplementary Figs. 4–9) obtained by an exploratory robot are sent to the laser-induced breakdown spectroscopy (LIBS) facility for elemental analysis (Supplementary Fig. 10). The robot carries out a set of physical and chemical pretreatment of ores needed for catalyst synthesis, including weighing (with a precision of 0.1 mg) in the solid-dispensing workstation, preparation of feedstock solutions in the liquid-dispensing and mixing workstations (Supplementary Table 1), separation from liquid in the centrifugation workstation and solidification in the dryer workstation. Then, the catalyst ink prepared by adding Nafion adhesive into the resulting metal hydroxides is used for making the working electrode

for electrochemical OER testing at the electrochemical workstation. Experimental data are sent to a cloud server for ML processing by the computational ‘brain’.

In the computational cycle, the ‘brain’ employs molecular dynamics (MD) simulations for tens of thousands of high-entropy hydroxides with different elemental ratios and applies density functional theory (DFT) calculations to estimate OER activities. Simulation data are used to train a theory-based neural network (NN) model for OER with varying elemental composition, which is soon re-trained and optimized with robot-driven experimental data. By embedding the optimized NN model in a Bayesian algorithm, the ‘brain’ predicts the best combination of available Martian ores for synthesizing an optimal OER catalyst, which is then verified experimentally by the AI chemist.

Building pretrained ML models using the computational ‘brain’

The OER is a thermodynamically uphill reaction involving four consecutive oxidation steps and O–O bond formation, which requires an applied voltage of no less than 1.23 V to operate. The OER overpotential, which is defined as the extra voltage above 1.23 V required for catalysis to occur, characterizes the voltage efficiency of the electrochemical device. Therefore, we chose the measured overpotential as the primary target of our ML model in searching for the optimal OER catalyst^{10–12}. We first created 29,902 unique compositions and simulated atomic structures of resulting high-entropy hydroxides (Fig. 2a) from classical MD simulations (Supplementary Figs. 11 and 12). The obtained structural features, such as averaged metal–metal and metal–oxygen distances (Supplementary Figs. 13 and 14 and Supplementary Table 2),

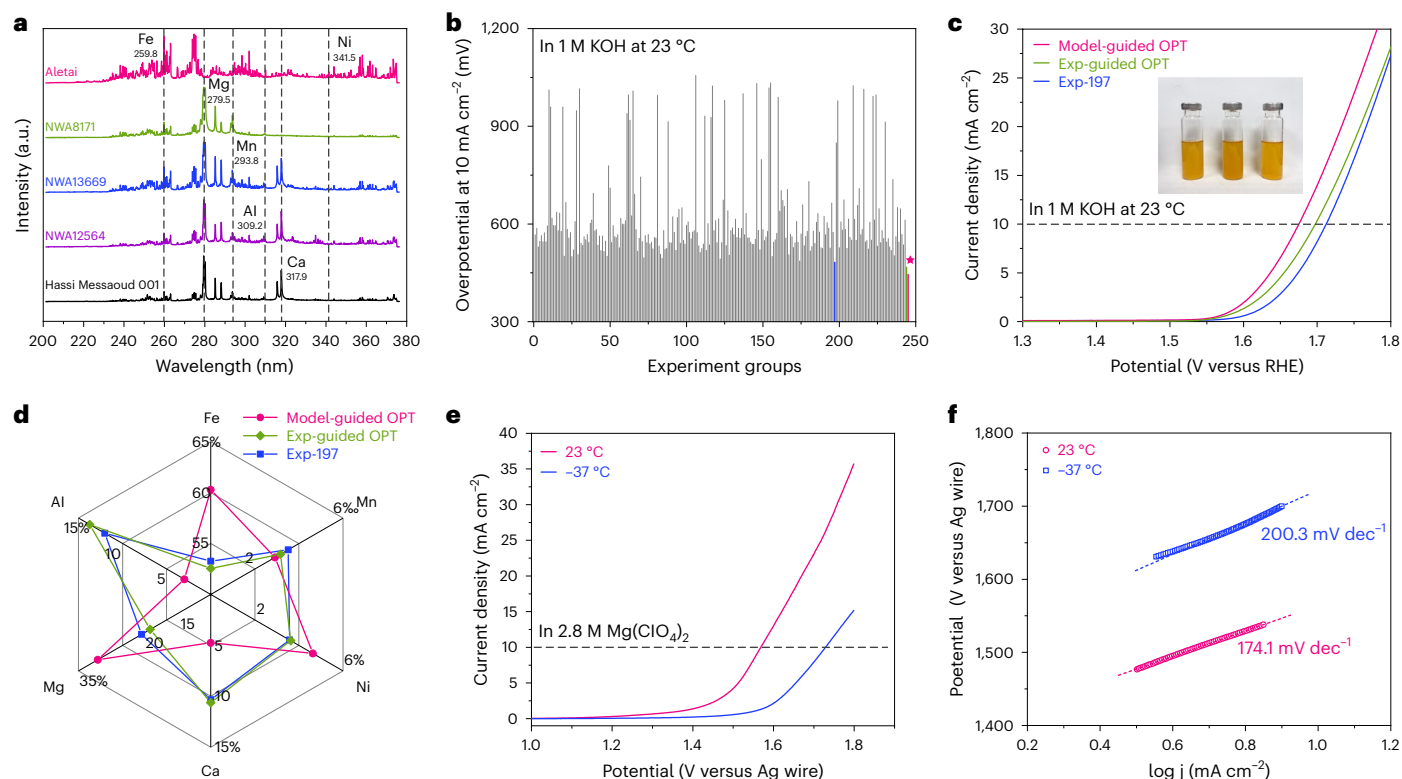


Fig. 3 | Searching for the best OER catalyst from Martian meteorites conducted by AI chemist. **a**, Representative LIBS spectral curves of five meteorite specimens in 200–380 nm with the ownership of main elemental emission lines. **b**, The η_{10} values of 243 ‘trial-and-error’ experiments performed by the mobile robot and workstations. The blue line indicates the best sample, ‘Experiment No. 197’ (in **c** and **d**, referred to as Exp-197), with the lowest overpotential among 243 pilot experiments; green line represents the catalyst obtained through experimental-data-guided local optimal search (in **c** and **d**, referred to as Exp-guided OPT); pink line demonstrates the result from Bayesian optimization using both simulated and experimental datasets (in **c** and **d**, referred to as Model-guided OPT). The pink star highlights the lowest

OER overpotential, suggesting that the ML model using both theoretical and experimental data achieves a global best synthetic formula, outperforming any other approach. **c**, LSV curves collected at a sweep rate of 5 mV s⁻¹ in 1 M KOH electrolyte. Insets are photographs of catalyst materials synthesized with components based on Martian meteorite composition, from left to right, Exp-197, Exp-guided OPT and Model-guided OPT. **d**, Kiviat diagram of elemental ratios. **e**, LSV curves of Model-guided OPT collected in CO₂-saturated 2.8 M Mg(ClO₄)₂ electrolyte at 23 °C and -37 °C, respectively. **f**, Corresponding Tafel plots for the anodic water oxidation derived from the LSV data in **e** to evaluate the reaction kinetics.

are passed to previously established bimetallic hydroxide models^{13,14} (Fig. 2b) to determine the OER activity of each multimetallic hydroxide by DFT calculation. Three DFT-predicted OER activity descriptors—including the Gibbs free energy change of hydroxyl adsorption ΔG_{OH^*} (ref. 15) and differences between the Gibbs free energy change for oxygen adsorption and hydroxyl adsorption $\Delta G_{\text{O}^*-\text{OH}^*}$ (ref. 16), the amount of charge transferred for hydroxyl adsorption on the activate site Δq (ref. 17)—and the paired composition information are used for NN training. As Fig. 2c shows, the NN model can accurately reproduce these DFT results. With the NN model, we can now rapidly predict the OER activity of high-entropy hydroxides obtained from any given composition of selected Martian ores (Supplementary Fig. 15), and these theoretical values are then connected with experimentally measured overpotentials. The ML model achieves remarkable accuracy in predicting true overpotentials (Fig. 2d).

High-throughput automated synthesis-characterization-performance optimization executed by the AI chemist

Using the LIBS-determined elemental composition of each Martian ore in Fig. 3a (here we use Martian meteorites to represent in situ Martian ores), the AI chemist prepared 243 different formulas with randomly selected compositions of six metal elements, performed electrocatalytic OER testing using each of them as catalyst and measured overpotentials by analysing linear sweep voltammetry (LSV) polarization

curves at a current density of 10 mA cm⁻² (η_{10}) per geometric area. The reason for choosing this specific current density is that it is approximately the current density expected at the anode of a 23% efficient solar-to-fuels conversion device under 1-sun illumination received on Mars^{18,19}. This preliminary screening generated an array of η_{10} values ranging from 482.2 to 1,056.2 mV (Fig. 3b). Then we trained the second NN model by using three computed OER activity descriptors and 243 sets of compositions as inputs and their corresponding experimental overpotentials as output (Fig. 2d). By concatenating these two NN models, the OER overpotentials for all 29,902 compositions can be easily predicted, creating a much larger dataset for Bayesian optimization¹⁰ to generate the optimal formula for a desired OER catalyst (Fig. 3c).

As the Kiviat plot indicates (Fig. 3d), the optimal compositions identified by the Bayesian model differ greatly from those of the best sample, namely Experiment No. 197 (Exp-197) from the pilot experiments, indicating that Bayesian optimization based on both simulated and experimental datasets can surpass experimental-data-guided local search. Meanwhile, the product with optimal composition predicted by the model that uses theoretical data also gives worse performance than the one from Bayesian optimization that relies on both simulated and experimental data (Supplementary Fig. 16). The catalyst with optimal composition (Model-guided OPT) was synthesized and verified by the AI chemist to have $\eta_{10} = 445.1$ mV, showing a substantial improvement (37.1 mV lower) with respect to the best result from a purely experimental search. Bayesian optimization suggested a metal

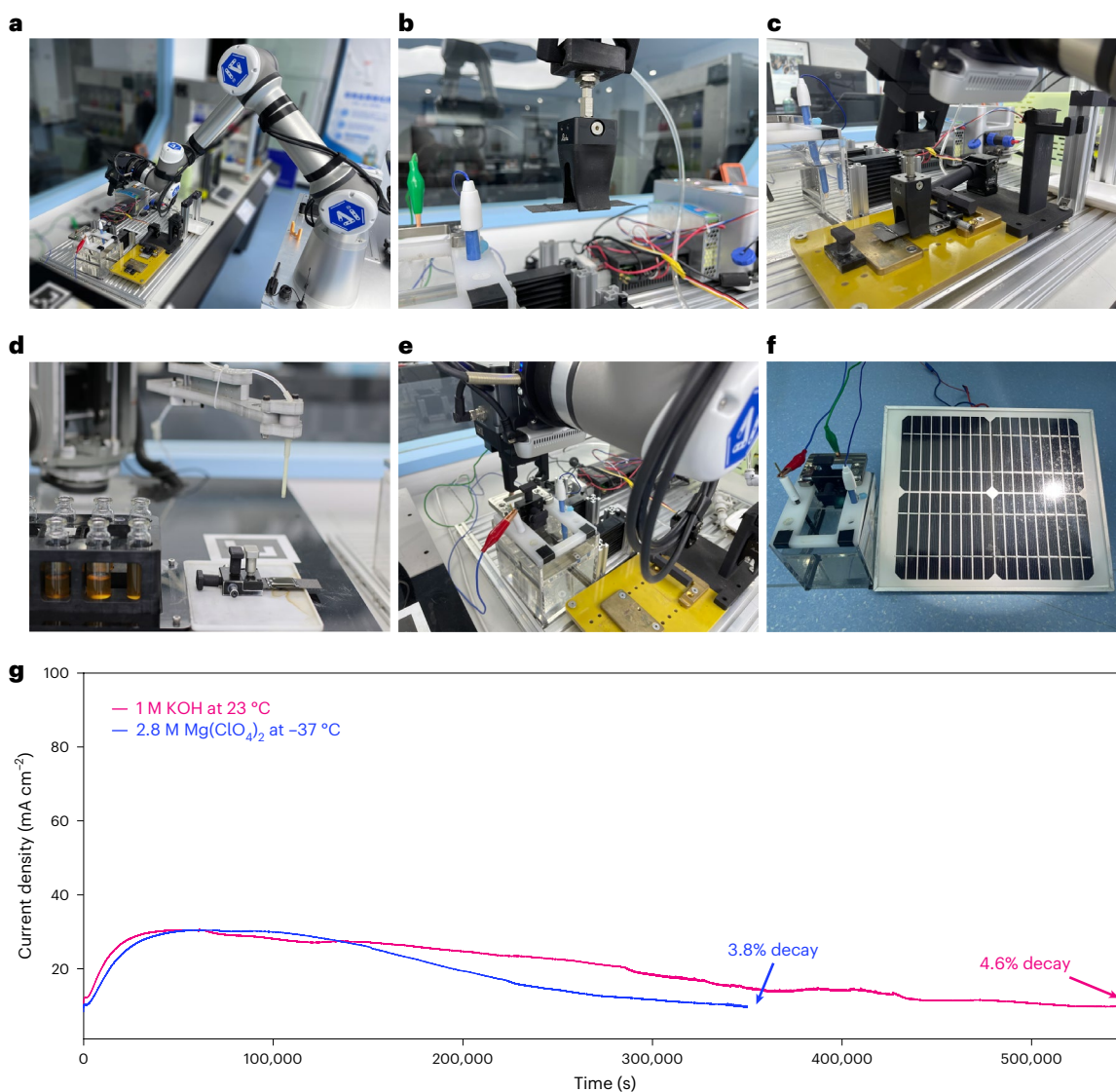


Fig. 4 | AI chemist completes the electrochemical measurement and evaluation of practical application potential of the catalyst derived from Martian meteorites. a, Positioning of the electrochemical workstation. **b,** Clamping of the carbon paper. **c,** Assembly of electrodes. **d,** Dripping of the catalyst ink. **e,** Placement of the working electrodes into the electrolyser.

f, Sunlight-driven OER process. **g,** The time-dependent current density curve of a Model-guided OPT sample on carbon-paper substrate acquired at working current density of 10 mA cm⁻² under 1 M KOH alkaline conditions at 23 °C and CO₂-saturated 2.8 M Mg(ClO₄)₂ electrolyte at -37 °C, respectively.

composition that was almost identical to that suggested by the grid point scanning in the simulation with the re-trained NN model, but with much less time consumption, suggesting that Bayesian optimization is more effective in finding a solution (Supplementary Table 3). For comparison, we also made a test using the experimental data only as input for Bayesian optimization. The resultant optimal composition of meteorites (Exp-guided OPT) gives $\eta_{10} = 467.4$ mV, which is very close to the best result among the 243 pilot experiments (Fig. 3d). Hence, the intrinsic limitation of local optimization with limited experimental data would likely be overcome by concatenating NN models trained from both theoretical and experimental data. After all, attempting to achieve the global best synthetic formula by exhaustive trial-and-error approach requires 3,764,376 possible experimental traversal searches (Supplementary Note 1), which is a nearly impossible task. The synthetic formulas of the several studied catalysts are listed in Supplementary Table 4, clearly and quantitatively comparing the differences in metal ratios among them. We also synthesized catalysts using only one meteorite as feedstock and found that

all performances were inferior to the local optimum solution found (Exp-197) (Supplementary Fig. 17).

After determining the optimal metal ratio with minimum overpotential, we performed detailed comparisons of other electrochemical parameters (Supplementary Figs. 18–20). We derived the trend of the reaction activation energy from the Tafel slope. The Model-guided OPT in 1.0 M KOH required a low value of only 61.35 mV dec⁻¹ to reach η_{10} , outperforming Exp-197 (83.59 mV dec⁻¹) and Exp-guided OPT (65.02 mV dec⁻¹) catalysts, indicating that it possesses a favourable kinetic process for an OER. The electrochemical surface area reflects the chemisorption capacity of the reacting substrate and the exposure of surface active sites. This parameter can be estimated by measuring the Helmholtz double-layer capacitance, allowing comparison of the intrinsic electrochemical activity of different catalysts²⁰. We found that the Model-guided OPT catalyst possesses the highest double-layer capacitance, which is about twice that of either the Exp-197 or Exp-guided OPT catalyst. This result implies that H₂O molecules can be in close contact with the surface of this catalyst and that both the input

of electrolyte and diffusion of the gaseous O₂ product are effectively accelerated. Electrochemical impedance spectroscopy is a technique that probes the internal processes of an electrochemical system and allows measurement of the operating state of the electrodes for kinetics study. By measuring the location and size of the semicircular region in the Nyquist plots, the voltages of solution and working electrode resistance losses can be obtained, which helps to analyse impedance changes as an aid in the assessment of electrocatalytic efficiency. We found that the semicircular diameters of the Exp-197, Exp-guided OPT and Model-guided OPT catalysts decrease sequentially, indicating that their charge transfer (or Faradaic) resistances follow the same trend.

Feasibility validation of oxygen production under simulated Martian environment

To verify the usability of catalysts under the low-temperature condition on the Martian surface, we performed an experiment based on the previous work of Gayen et al.¹ and the fact that large-scale water resources have been found in the Martian regolith^{21,22}. The operating conditions on the Martian surface were constructed with a 2.8 M Mg(ClO₄)₂ brine solution as the electrolyte, platinum mesh as counter electrode and robust Ag wire as the reference at 23 °C and -37 °C (Fig. 3e). The LSV polarization curves suggest low voltage values of 1.5685 V and 1.7289 V to reach the current density of 10 mA cm⁻² with Tafel slopes of 174.1 mV dec⁻¹ and 200.3 mV dec⁻¹, respectively (Fig. 3f and Supplementary Fig. 21).

Long-term stability is crucially important for the practical application of OER catalysts. We performed cycling stability tests on the catalyst under various conditions by applying a certain voltage to the catalyst working electrode and assembling the electrolyser to maintain its initial oxygen production current at 10 mA cm⁻² in a classical three-electrode system (Fig. 4a–f). Prolonged testing showed that the as-prepared Model-guided OPT catalyst works steadily at the current density of 10 mA cm⁻² for more than 550,000 s (-153 h) in 1 M KOH at 23 °C and 350,000 s (-97 h) in 2.8 M Mg(ClO₄)₂ brine solution at -37 °C (Fig. 4g), indicating that this AI-chemist-designed catalyst is as stable as other state-of-the-art OER catalysts. It can also be estimated that in 1 M KOH, the catalyst made by AI chemist can achieve an average O₂ production rate of 59.08 g h⁻¹ m⁻². For a Martian station room with 300 m³ volume (100 m² area and 3 m height) coated with the produced OER catalyst film on its roof, it will take about 15.2 h to achieve oxygen self-sufficiency. This process could be accelerated with the catalyst directly grown on the conductive nickel foam substrate as it is synthesized, which maintains considerably efficient and stable O₂ production capability at an even higher current density condition (Supplementary Fig. 22), albeit requiring larger area solar panels to generate more electricity to boost the OER reaction. It is likely that given more types of metal elements in Martian ores and advanced mineral refining facilities, the performance of Mars-mineral-derived chemicals and materials can be further improved in the future.

Conclusion

Our study provides a demonstration that an advanced AI chemist can, without human intervention, synthesize OER catalysts on Mars from local ores. This system has demonstrated its ability to perform all required experimental steps, including raw material analysis, pretreatment, synthesis, characterization and performance testing with high precision and also shown its intelligent analysis power in identifying the best formula for a Martian OER catalyst from millions of possible combinations. Particularly powerful is the in situ optimization, which seamlessly combines the experimental data and computational data during the synthesis process, greatly accelerating the generation of a reliable model and finding of an optimal formula. The established protocol and system, which are generic and adaptive, are expected to advance automated material discovery and synthesis of chemicals for the occupation and exploration of extraterrestrial planets.

Methods

Chemicals and materials

NaOH (99.9%), KOH (99.9%), HCl (37% trace metals), K₃[Fe(CN)₆] (99%), K₄[Fe(CN)₆]·3H₂O (99.5%), anhydrous ethanol and 5 wt% Nafion 117 solution were purchased from Sigma-Aldrich. The counter electrode of graphite rod and reference electrodes of Ag/AgCl in saturated KCl were purchased from CH Instruments. The deionized water (18.2 MΩ cm⁻¹) used for the feedstocks solution and aqueous electrolytes preparation were made with a Milli-Q EQ 7000 Ultrapure water purification system.

Catalyst synthesis

Five different categories of meteorites that come from or have been confirmed to exist on Mars were selected^{23,24}; complete information describing these approved meteorites can be found on the website of the Meteoritical Bulletin Database available at <http://www.lpi.usra.edu/meteor/>. We digested various masses of these individual meteorites in 1 mol l⁻¹ hydrochloric acid solution based on the results of elemental analysis by a LIBS spectrometer, which was used to configure the feedstocks solution to control the total mass concentration of the six key catalytic metals (that is, Fe, Mn, Ni, Ca, Mg and Al) to 200 mg l⁻¹. For the catalyst preparation, the AI chemist set the addition amount of total feedstocks solution to reaction vial to 10 g at the liquid-dispensing workstation, but randomly varied the proportion of each feedstock entered. In this manner, the atomic ratio of metals in the final product can be finely adjusted. Afterwards, 3 g of aqueous NaOH solution with a concentration of 4 mol l⁻¹ was added to the reaction vials and stirred for 5 minutes, followed by centrifugation at 7,500g for 5 minutes, aspiration of the upper waste solution, washing with anhydrous ethanol and drying at 60 °C. The described synthetic procedure was done to perform the initial search for the optimal metal ratio in a catalyst and was performed for 243 groups of experiments. During the whole process, the intelligent 'brain' of the AI-chemist system automatically generates .xml execution files and sends them to the experimental robot, which—with various synthesis and testing workstations—sequentially automates the preparation of the catalyst material. Similarly, the synthesis of samples Exp-guided OPT and Model-guided OPT is based on the same method as above, except that the respective metal ratios are determined and given by the intelligence 'brain' and converted by a transformation matrix.

Analysis of metal content in meteorites by LIBS

LIBS is a rapid chemical analysis technology that offers many compelling advantages compared to other elemental analysis techniques in geoscience. The main physical process that constitutes the essence of LIBS technology is the formation of a high-temperature plasma created by ultrafast laser pulses (UFLPs). When the UFLP beam is focused on the surface, a small portion of sample mass is ablated, a process called laser ablation. This ablated mass further interacts with the trailing portion of the UFLP to form a short-lived high-temperature plasma containing free electrons, excited atoms and ions. When the laser pulse is terminated, the plasma cools and the electrons in atoms or ions at the excited state decay to their natural ground state. Correspondingly, the wavelengths of the emitted photons are inversely proportional to the energy difference between the excited and ground states, so that each element has its own set of characteristic emission wavelengths, a fingerprint signature, which is then collected and coupled to the spectrometer detector module for LIBS spectroscopy. Each element in the periodic table is associated with a unique LIBS spectral peak. The high energy density of the focused UFLP allows the excitation of material in any physical state (in our case, solid) to form a plasma, allowing the LIBS technique to analyse samples and assess the relative abundance of each constituent element.

Our LIBS workstation consists of a researcher-developed sample feed system, a nanosecond laser generator (Quantel Viron), a fibre-optical spectrometer (AvaSpec-ULS2048CL-2-EVO), an optical system

and a high-performance computer. The feed system consists of a motorized delivery track, a slowly rotating sample stage and a motor control unit. The control unit is designed independently, with the main control chip being the Atmel-produced MEGA 2560V chip. The robotic arm of the AI chemist places the sample on the stage, which is then delivered by the feed system for laser irradiation with slow rotation so that different points on the surface are excited by the laser to obtain an unattenuated signal. The pulsed laser emitted from the laser generator is focused on the sample surface by the optical system to produce a transient high-temperature plasma. The signal is captured by the optical fibre of the spectrometer. A researcher-written programme in the computer controls the measurement process automatically and acquires spectral data from the spectrometer for subsequent analysis and processing.

The LIBS spectra were collected under optimized conditions: laser pulse energy, 105 mJ; spot diameter, 2 mm; spectrometer slit width, 15 mm; gate width, 1 ms and acquisition delay, 180 ms. In total, 388 sets of data points were obtained, these spectra were accumulated, and then the peak line region of the target element was marked according to the elemental peak lines obtained from the NIST database (https://physics.nist.gov/PhysRefData/ASD/lines_form.html) and the baseline correction was performed for peak line region. After wavelet filtering, the best Lorentz peak shape and the offset of the actual peak line relative to its standard spectrum were obtained by fitting with the Levenberg–Marquadt method. Here, the half-height width of the peak, the wavelength of crest and the signal intensity were used as intrinsic characteristics. The preliminary elemental content was calculated by linear regression. Subsequently, the top 50 data points in the original spectrum with the highest correlation with the elemental content (found by the LASSO algorithm after normalization from the pretraining set data) are transformed in the same way as the pretraining set data and then entered into a pretrained backpropagation NN together with the preliminary content calculated in the previous step to obtain a more accurate elemental content. Similarly, the above analysis is repeated for each targeted element to obtain the exact content with a relative error within $\pm 5\%$.

Transfer metals molar ratio to Martian ores mass ratio

The feedstock solutions are prepared by the following procedure: Take out 271.05 mg of Aletai, 567 mg of NWA 8171, 563.2 mg of NWA 13669, 935 mg of NWA 12564, 688.5 mg of Hassi Messaoud 001, each dissolved in 1 l of acidic solution to prepare the feedstock solution for the experiments. In this way, the total mass concentrations of metal ions in all feedstock solutions are controlled at about 200 mg l^{-1} ; the concentrations of metals are listed in Supplementary Table 1.

Because the ML-model-predicted results are the metal molar ratios, we prepared a researcher-developed software programme to transfer metals molar ratio to Martian ores mass ratio for convenient robotic weighting operation. The software is developed using Python, and it is also converted to a windows-based executable programme (Supplementary Fig. 15). The source code is as follows:

```
import tkinter as tk
import numpy as np
from scipy.linalg import solve
window = tk.Tk()
window.title('Transfer ratio')
window.geometry('500x750')

s1 = tk.Label(window, text = 'Fe')
s1.pack()
a1 = tk.Entry(window, show=None)
a1.pack()

s2 = tk.Label(window, text = 'Mn')
s2.pack()
```

```
a2 = tk.Entry(window, show=None)
a2.pack()
```

```
s3 = tk.Label(window, text = 'Ni')
s3.pack()
a3 = tk.Entry(window, show=None)
a3.pack()
```

```
s4 = tk.Label(window, text = 'Ca')
s4.pack()
a4 = tk.Entry(window, show=None)
a4.pack()
```

```
s5 = tk.Label(window, text = 'Mg')
s5.pack()
a5 = tk.Entry(window, show=None)
a5.pack()
```

```
s6 = tk.Label(window, text = 'Al')
s6.pack()
a6 = tk.Entry(window, show=None)
a6.pack()
```

```
def transfer():
```

```
    b1 = a1.get()
    b2 = a2.get()
    b3 = a3.get()
    b4 = a4.get()
    b5 = a5.get()
    b6 = a6.get()
```

```
    metal_ratio = np.array([float(b1), float(b2), float(b3), float(b4), float(b5), float(b6)])
```

```
    abundance = np.array([[3.303, 0.0328, 0.0055, 0.00155, 0.00149],
    [1.379, 0.0288, 0.01374, 5.167, 0.02],
    [2.4, 0.0521, 0.07697, 1.306, 0.0803],
    [0.97, 0.0132, 0.1417, 0.744, 2.759],
    [2.238, 0.0541, 0.1142, 1.438, 0.0779]])
```

```
    transfer_matrix = abundance.T
```

```
    meteorite_ratio = solve(transfer_matrix[0:5], metal_ratio[0:5])
```

```
    meteorite_ratio = meteorite_ratio/sum(meteorite_ratio)
```

```
    abcdelist = [0.27105, 0.567, 0.5632, 0.935, 0.6885]
```

```
    meteorite_ratio = meteorite_ratio*10*abcdelist
```

```
    meteorite_ratio = meteorite_ratio.round(4)
```

```
    result = ''.join(str(i) for i in meteorite_ratio)
```

```
    t.insert('insert', meteorite_ratio (A,B,C,D,E) is: '+result + '\n')
```

```
button = tk.Button(window,
    text = 'Transfer',
    width=15, Height=2,
    command=transfer,)
button.pack()
```

```
t = tk.Text(window)
t.pack()
window.mainloop()
```

OER measurement under 1 M KOH alkaline condition

All the electrochemical measurements were conducted at the electrochemical workstation (CHI660E, CH Instruments) in a standard three-electrode setup with the catalyst derived from Martian meteorites as the working electrode, a graphite rod as the counter electrode and Ag/AgCl in saturated KCl as reference electrode. All the electrocatalytic OER performance was studied under alkaline conditions (1 mol l^{-1} KOH). The applied potential was calibrated to reversible hydrogen electrode (RHE) following the equation $E_{\text{RHE}} = E_{\text{Ag/AgCl}} + 0.0591 \times \text{pH} + 0.197 \text{ V}$.

Unless otherwise specified, neither iR-compensation nor background current correction was applied. For the working electrode preparation, the as-prepared catalyst dispersing in 5 ml of a mixed solution of ethanol (4.8 ml) and 5 wt% Nafion (0.2 ml) under magnetic stirring to form a uniform catalyst ink. Then, 200 μl of the resulting catalyst ink was drop-casted onto a carbon paper with the loading area of $2.5 \times 2 \text{ cm}^2$, and the corresponding final metal loading was calculated to be 0.08 mg cm^{-2} . Cyclic voltammetry activation curve was performed 40 times from 1.0 V to 1.5 V with respect to the RHE reference at a sweep rate of 50 mV s^{-1} . LSV measurements were performed from 1.0 V to 2.0 V with respect to the RHE reference at a scan rate of 5 mV s^{-1} . Tafel slope (b) is obtained by fitting the linear portion according to the Tafel equation ($\eta = a + b \log(j)$) using the overpotential (η) as a function of the logarithmic scale of current density ($\log(j)$). Electrochemical impedance spectroscopy measurements performed at an overpotential of 0.4 V for working electrodes. Electrochemical active surface areas are evaluated based on the double-layer capacitance via the analysis of a series of cyclic voltammetry measurements performed within the non-Faradaic potential region (1.05 to 1.15 V with respect to the RHE reference) at various scan rates (10, 20, 40, 60, 80, 100, 120, 140, 160, 180 and 200 mV s^{-1}). The chronoamperometry ($i-t$) test was collected at a constant potential at 1.7 V with respect to the RHE reference for 550,000 seconds. All the electrochemical characterizations can be performed automatically by one-click measurements and generate the experimental reports using a researcher-written Python code. To grow the catalyst on nickel foam substrate for oxygen production at industrial current density, we added feedstocks solution prepared from five Martian meteorites to the autoclave reactor, followed by NaOH addition to adjust the pH to 5–6, then 0.2 g of urea was added to dissolve, and finally cleaned nickel foam with thickness of 2 mm was placed vertically, encapsulated and held at $130 \text{ }^\circ\text{C}$ for 10 hours. When the reaction is completed, the nickel foam is taken out, washed and dried for OER performance testing in compliance with the described three-electrode system.

In situ electrocatalytic oxygen generation experiments under simulated Martian surface environmental conditions

As the Martian surface is well below $0 \text{ }^\circ\text{C}$ for most of the Mars year and its atmosphere is rich in CO_2 , we used aqueous $\text{Mg}(\text{ClO}_4)_2$ solution ($\text{pH} \approx 7$) with a concentration of 2.8 M as a mimic of the brine solution already explored on Mars and then used a dry ice solution of ethanol-ethylene glycol mixture at a constant temperature of $-37 \text{ }^\circ\text{C}$ for OER testing²⁵. Considering such a low temperature, the conventional Ag/AgCl electrode is no longer suitable as a reference; therefore, we used Ag wire (99.99%, $\phi = 1.5 \text{ mm}$) as a reference electrode at low-temperature conditions and potassium ferrocyanide-potassium ferricyanide oxidation-reduction potential buffer as internal standard to determine the potential of Ag wire at approximately 0.427 V with respect to an RHE reference. All electrochemical test steps and data processing procedures are similar to those performed in 1 M KOH, except that the corresponding voltage window is changed and the $\text{Mg}(\text{ClO}_4)_2$ solution is saturated with CO_2 (99.999%) prior to testing.

Theoretical calculations

MD simulations. To extract structural features of high-entropy hydroxides, we sampled one million equilibrated structures for each of 29,902 unique formulas of six-metallic elements (Fe, Ni, Mn, Ca, Mg and Al) using classical MD simulation. The initial configuration of each composition was generated by randomly placing 60 different metal cations and the corresponding number of hydroxyl anions for maintaining neutrality into a cubic box of $3 \times 3 \times 3 \text{ nm}^3$ using GROMACS²⁶. The universal force field²⁷ was adopted and all parameters for high-entropy hydroxides were generated by the LAMMPS Interface programme²⁸. The cutoff distances for both Lennard–Jones and Coulombic potential were set to be 12.5 \AA . Then, each initial structure was pre-equilibrated by energy minimization. In a production MD run, a trajectory of 1 ns

with a time step of 1 fs was collected in an NPT ensemble with $P = 1 \text{ atm}$ and $T = 2,000 \text{ K}$ using the Nosé–Hoover barostat and thermostat^{29,30}. For each trajectory, we retrieved 100 configurations in an evenly divided 10 ps interval and computed averaged metal–metal and metal–oxygen distances as structure features of these high-entropy hydroxides. All force field base simulations were carried out with the LAMMPS package³¹.

DFT calculation. To describe the OER activity of high-entropy hydroxides, DFT calculations on the simplified bimetallic hydroxide model with the information of statistical structure features of each unique composition embedded were performed using the Perdew–Burke–Ernzerhof functional³² and the projector augmented wave method³³ as implemented in the Vienna ab initio simulation package³⁴. The kinetic energy cutoff of the plane-waved basis set was 400 eV. The Brillouin zone was sampled with $3 \times 2 \times 1$ Monkhorst–Pack k-mesh with the vacuum size chosen to be 15 \AA to avoid interaction between two layers for all structures. The long-range van der Waals interaction corrections were described using Grimme’s D3 correction³⁵. All geometry but the metal–(η^2 -oxygen)₂–metal moiety is allowed to relax. The convergences of total energy for wave function self-consistency and force between atoms for optimization were set to be 10^{-5} eV and 0.01 eV \AA^{-1} , respectively.

Calculation for the free energies. The Gibbs free energies ΔG_{OH^*} and $\Delta G_{\text{O}^*-\text{OH}^*} = \Delta G_{\text{O}^*} - \Delta G_{\text{OH}^*}$ and Δq (the amount of charge transferred for hydroxyl adsorption on the activate site) were used as computational descriptors of OER activity. For all possible combinations of dual metal atoms in every high-entropy hydroxide, their OER descriptors were calculated using the following procedure.

The elementary steps of hydroxyl adsorption and oxygen adsorption can be given as:



Under zero potential, the Gibbs free energy of each elementary step was given by the expression:

$$\Delta G = \Delta E + \Delta \text{ZPE} - T\Delta S$$

where ΔE is the change in reaction energy. The ΔZPE is the zero-point energy change, and ΔS is the entropy change for each elementary step with the temperature at 298.15 K.

NN architecture

The first NN model—which uses information of metal composition as input and the DFT calculated three catalytic properties (ΔG_{OH^*} , $\Delta G_{\text{O}^*-\text{OH}^*}$, Δq) as output—comprises one input layer, two hidden layers and one output layer. The number of neurons in both hidden layers is 512. To link computed catalytic properties and experimentally measured overpotential, the second NN model was built with one input layer, three hidden layers involving 128 neurons each and one output layer. For the training of each NN, the dataset was divided into two subsets, one for training (80%) and the other for testing (20%). The NN model was trained with a backpropagation algorithm and the Rectified Linear Unit activation function³⁶ as implemented in TensorFlow³⁷.

Two NNs were combined to create a predicting model that used the metal composition as a descriptor to estimate the real overpotential. A Bayesian approach, taking above predicting model as objective function, was then applied to identify the optimal metal composition with the highest catalytic activity. The Bayesian optimization loop consisted of 280 iterations, and the surrogate model was a basic Gaussian process, which could capture the uncertainty and noise in the data

and handle different types of objective functions. We also used the upper confidence bound as our acquisition function, which balanced exploration and exploitation by adding a positive term depending on the standard deviation to the mean estimate of the objective function.

Data availability

The data that support the findings of this study are available in the paper, its Supplementary Information and Supplementary Video I.

Code availability

The code used for training an NN model for OER prediction with theoretical data and robot-driven experimental data is available on GitHub at <https://github.com/Lulu971231/code-for-Oxygen-Producing-Catalysts-from-Martian-Meteorites>.

References

1. Gayen, P., Sankarasubramanian, S. & Ramani, V. K. Fuel and oxygen harvesting from Martian regolithic brine. *Proc. Natl Acad. Sci. USA* **117**, 31685–31689 (2020).
2. Hoffman, J. A. et al. Mars Oxygen ISRU Experiment (MOXIE)—preparing for human Mars exploration. *Sci. Adv.* **8**, eabp8636 (2022).
3. Wade, J., Dyck, B., Palin, R. M., Moore, J. D. P. & Smye, A. J. The divergent fates of primitive hydrospheric water on Earth and Mars. *Nature* **552**, 391–394 (2017).
4. Orosei, R. et al. Radar evidence of subglacial liquid water on Mars. *Science* **361**, 490–493 (2018).
5. Kruyer, N. S., Realff, M. J., Sun, W., Genzale, C. L. & Peralta-Yahya, P. Designing the bioproduction of Martian rocket propellant via a biotechnology-enabled in situ resource utilization strategy. *Nat. Commun.* **12**, 6166 (2021).
6. Yao, Y. et al. Extraterrestrial photosynthesis by Chang'E-5 lunar soil. *Joule* **6**, 1008–1014 (2022).
7. Burger, B. et al. A mobile robotic chemist. *Nature* **583**, 237–241 (2020).
8. Rohrbach, S. et al. Digitization and validation of a chemical synthesis literature database in the ChemPU. *Science* **377**, 172–180 (2022).
9. Zhu, Q. et al. An all-round AI-chemist with a scientific mind. *Natl Sci. Rev.* **9**, nwac190 (2022).
10. Pyzer-Knapp, E. O., Chen, L., Day, G. M. & Cooper, A. I. Accelerating computational discovery of porous solids through improved navigation of energy-structure-function maps. *Sci. Adv.* **7**, eabi4763 (2022).
11. Butler, K. T., Davies, D. W., Cartwright, H., Isayev, O. & Walsh, A. Machine learning for molecular and materials science. *Nature* **559**, 547–555 (2018).
12. Sanchez-Lengeling, B. & Aspuru-Guzik, A. Inverse molecular design using machine learning: generative models for matter engineering. *Science* **361**, 360–365 (2018).
13. Bai, L., Hsu, C.-S., Alexander, D. T. L., Chen, H. M. & Hu, X. Double-atom catalysts as a molecular platform for heterogeneous oxygen evolution electrocatalysis. *Nat. Energy* **6**, 1054–1066 (2021).
14. Lin, C. et al. In-situ reconstructed Ru atom array on α -MnO₂ with enhanced performance for acidic water oxidation. *Nat. Catal.* **4**, 1012–1023 (2021).
15. Xu, H., Cheng, D., Cao, D. & Zeng, X. C. A universal principle for a rational design of single-atom electrocatalysts. *Nat. Catal.* **1**, 339–348 (2018).
16. Craig, M. J. et al. Universal scaling relations for the rational design of molecular water oxidation catalysts with near-zero overpotential. *Nat. Commun.* **10**, 4993 (2019).
17. Tao, L. et al. Charge transfer modulated activity of carbon-based electrocatalysts. *Adv. Energy Mater.* **10**, 1901227 (2020).
18. Walter, M. G. et al. Solar water splitting cells. *Chem. Rev.* **110**, 6446–6473 (2010).
19. Appelbaum, J. & Flood, D. J. Solar radiation on Mars. *Sol. Energy* **45**, 353–363 (1990).
20. McCrory, C. C. L., Jung, S., Peters, J. C. & Jaramillo, T. F. Benchmarking heterogeneous electrocatalysts for the oxygen evolution reaction. *J. Am. Chem. Soc.* **135**, 16977–16987 (2013).
21. Hecht, M. H. et al. Detection of perchlorate and the soluble chemistry of Martian soil at the Phoenix lander site. *Science* **325**, 64–67 (2009).
22. Cull, S. C. et al. Concentrated perchlorate at the Mars Phoenix landing site: evidence for thin film liquid water on Mars. *Geophys. Res. Lett.* **37**, L22203 (2010).
23. Schröder, C. et al. Meteorites on Mars observed with the Mars exploration rovers. *J. Geophys. Res.* **113**, E06S22 (2008).
24. Ashley, J. CosmoELEMENTS: the study of exogenic rocks on Mars—an evolving subdiscipline in meteoritics. *Elements* **11**, 10–11 (2015).
25. Jensen, C. M. & Lee, D. W. Dry-ice bath based on ethylene glycol mixtures. *J. Chem. Educ.* **77**, 629 (2000).
26. Abraham, M. J. et al. GROMACS: high performance molecular simulations through multi-level parallelism from laptops to supercomputers. *SoftwareX* **1–2**, 19–25 (2015).
27. Mayo, S. L., Olafson, B. D. & Goddard, W. A. DREIDING: a generic force field for molecular simulations. *J. Phys. Chem.* **94**, 8897–8909 (1990).
28. Boyd, P. G., Moosavi, S. M., Witman, M. & Smit, B. Force-field prediction of materials properties in metal-organic frameworks. *J. Phys. Chem. Lett.* **8**, 357–363 (2017).
29. Nosé, S. A unified formulation of the constant temperature molecular dynamics methods. *J. Chem. Phys.* **81**, 511–519 (1984).
30. Hoover, W. G. Canonical dynamics: equilibrium phase-space distributions. *Phys Rev A (Coll Park)* **31**, 1695–1697 (1985).
31. Plimpton, S. Fast parallel algorithms for short-range molecular dynamics. *J. Comput. Phys.* **117**, 1–19 (1995).
32. Perdew, J. P., Burke, K. & Ernzerhof, M. Generalized gradient approximation made simple. *Phys. Rev. Lett* **77**, 3865–3868 (1996).
33. Blöchl, P. E. Projector augmented-wave method. *Phys. Rev. B* **50**, 17953–17979 (1994).
34. Kresse, G. & Furthmüller, J. Efficiency of ab-initio total energy calculations for metals and semiconductors using a plane-wave basis set. *Comput. Mater. Sci.* **6**, 15–50 (1996).
35. Grimme, S., Ehrlich, S. & Goerigk, L. Effect of the damping function in dispersion corrected density functional theory. *J Comput. Chem.* **32**, 1456–1465 (2011).
36. Maas, A. L., Hannun, A. Y. & Ng, A. Y. Rectifier nonlinearities improve neural network acoustic models. In *Proc. 30th International Conference on Machine Learning (ICML)* (eds Dasgupta, S. & McAllester, D.) 3 (ACM Press, 2013).
37. Abadi, M. et al. TensorFlow: a system for large-scale machine learning. In *Proc 12th USENIX Conference on Operating Systems Design and Implementation* (eds Keeton, K. & Roscoe, T.) 265–283 (USENIX Association, 2016).

Acknowledgements

Y.L. acknowledges funding support for this research from the Innovation Program for Quantum Science and Technology (Grant 2021ZD0303303). J.J. gratefully acknowledges financial support by the National Natural Science Foundation of China (Grants 22025304, 22033007) and the CAS Project for Young Scientists in Basic Research (Grant YSBR-005). Q.Z. gratefully acknowledges the financial support of the National Natural Science Foundation of China (Grant 22103076) and Anhui Provincial Natural Science Foundation (Grant 2108085QB63). We also gratefully acknowledge the USTC Center for Micro- and Nanoscale Research and Fabrication for providing

experimental resources and the USTC supercomputing centre for providing computational resources.

Author contributions

These authors contributed equally: Q.Z., Y.H., D.Z., L.Z. Q.Z. planned and conducted the robotic experiments and collected and analysed the experiment data. Y.H., D.Z., L.Z. and H.L. performed theoretical simulations and ML training. L.G., R.Y., Z.S. and M.L. assisted with the spectroscopic characterization and data analysis. H.X., B.Z. and J.C. were responsible for writing test scripts. X.T. and Y.Z. contributed to the development of robotic operation module, robotic arm motion planning and force control. J.Z. and B.C. helped with the robot platform communication, SLAM, platform motion planning and navigation. T.S. planned robot movement and operation task management system. X.L. and S.C. managed the scheduling optimization of robot experimental tasks at various workstations. X.Z. developed the robotic visual localization algorithm. F.Z. and W.S. designed the entire robot system. G.Y. and W.Z. worked on non-standardized equipment development. S.W., G.Z. and H.Z. contributed to the original draft preparation. L.-L.L. and Z.Z. assisted in the design and execution of experiments under simulated Martian environments. J.J. and Y.L. conceptualized the study, developed the methodology and conducted the investigation and wrote, reviewed and edited the paper. All authors participated in discussions and revisions and provided comments on the paper.

Competing interests

The authors declare no competing interests.

Additional information

Supplementary information The online version contains supplementary material available at <https://doi.org/10.1038/s44160-023-00424-1>.

Correspondence and requests for materials should be addressed to Weiwei Shang, Jun Jiang or Yi Luo.

Peer review information *Nature Synthesis* thanks Leroy Cronin, Zhigang Zou and the other, anonymous, reviewer(s) for their contribution to the peer review of this work. Primary Handling Editor: Peter Seavill, in collaboration with the *Nature Synthesis* team.

Reprints and permissions information is available at www.nature.com/reprints.

Publisher's note Springer Nature remains neutral with regard to jurisdictional claims in published maps and institutional affiliations.

Springer Nature or its licensor (e.g. a society or other partner) holds exclusive rights to this article under a publishing agreement with the author(s) or other rightsholder(s); author self-archiving of the accepted manuscript version of this article is solely governed by the terms of such publishing agreement and applicable law.

© The Author(s), under exclusive licence to Springer Nature Limited 2023